Met. Mater. Int., Vol. 20, No. 6 (2014), pp. 1067~1071
doi: 10.1007/s12540-014-6010-x

SIMS Evaluation of Poly Crystal Boron Nitride Tool Effect in Thermo-Mechanically Affected Zone of Friction Stir Weld Steels

JaeNam Kim[1,3], SangUp Lee[2], HyoegDae Kwun[2], KwangSoo Shin[2], and ChangYong Kang[3,*]

[1]POSTECH, Graduate Institute of Ferrous Technology, Pohang 790-784, Korea
[2]RIST,Center for Analysis and Assessment, Pohang 790-330, Korea
[3]Pukyong National University, Department of Metallurgical Engineering, Busan 608-739, Korea

(received date: 5 August 2013 / accepted date: 10 February 2014)

The effect of the poly crystal boron nitride (PCBN) tool in friction stir weld (FSW) steels was evaluated using the secondary ion mass spectroscopy (SIMS) technique. This study focused on the quantitative SIMS analysis of impurity boron through a resistive anode encoder (RAE) image. The RAE images were transformed retrospective depth profile by profiler. The relative sensitivity factors (RSFs) for boron varied heavily according to by the polarity of secondary voltage and matrix materials. The RAE images of cluster-polyatomic secondary ion species, $^{11}B^{16}O_2$, properly map the distribution of impurity boron in the thermo-mechanically affected zone (TMAZ) of FSW steels using negative secondary polarity 4.5 kV. A combination of cluster-polyatomic ion, $^{11}B^{16}O_2$ and $^{56}Fe^{16}O$ provided a good calibration curve by 3 SRMs with the least matrix effect. The boron concentrations of TMAZ in FSW steels were determined through the calibration curve by taking the corresponding boron concentration value (C_B) of the intensity ratio (I_i/I_m) from unknown samples. The new SIMS quantification technique of impurity boron from RAE images is found to be effective for a more quantitative understanding of the wear mechanism of the PCBN tool in TMAZ of FSW steels.

Keywords: friction stir weld (FSW), poly crystal boron nitride (PCBN) tool, secondary ion mass spectrometry (SIMS), boron quantification, thermo-mechanically affected zone (TMAZ)

1. INTRODUCTION

Friction stir weld (FSW) is a solid-state joining process that uses a rotating tool to join faying surfaces. Heat is generated between the tool and material which leads to a very soft region due to the elevated temperature. It then mechanically intermixes the two pieces of metal at the place of the join, and then the softened metal can be joined using mechanical pressure which is applied by the tool. The microstructure and mechanical properties of FSW joints depend on the base materials and FSW parameters including tool materials [1-3]. Poly crystal boron nitride (PCBN) is the preferred tool materials for FSW of hard alloys such as steels because of its high strength and hardness at elevated temperatures along with high temperature stability. Also, the low coefficient of friction for PCBN results in a smooth weld surface. One research results on the wear properties of PCBN, which is not as a welding tool, but as a cutting tool has shown that abrasion and diffusion are the wear mechanism [4]. However, these wear mechanisms are relevant to the FSW process. Tool wear affect not only the tool life but also weld characteristics. This study focused on the quantitative comparison of impurity boron between two different contrasts of thermo-mechanically affected zone (TMAZ) of FSW steel which might be related to wear mechanism.

Secondary ion mass spectroscopy (SIMS) is an analytical technique that can be used to characterize the surface and near surface region of solids. One of the advantages of SIMS is the outstanding impurity detection limits of part per million atomic for most elements. However, SIMS quantification is subject to many effects. Not only the matrix effect of the analyzed materials but also the physics of the sputtering process will often affect the interpretation of the data. The relative sensitivity factor (RSF) is a conversion factor from secondary ion intensity to atom density for the quantification. Many calibration runs have to be performed for each element and each type of sample matrix to obtain relevant sets of RSF. One more important thing is that the experimental conditions and sample preparation have to be well controlled and identical in the calibration runs and the actual analysis runs in order to obtain reliable data. Practically RSF has a great variation result from the analytical parameters and sample materials. The authors found that the use of clus-

*Corresponding author: metkcy@pknu.ac.kr

ter type polyatomic secondary ion species can reduce the matrix effect significantly [5].

2. EXPERIMENTAL PROCEDURES

Table 1 gives the chemical composition of the standard reference materials (SRMs) used in this study. The SRMs are ready-made from the National Institute of Standard and Technology (NIST, USA) for emission spectrometry which is commonly used for precise chemical quantification in the steel industry. It should be noted, however, that these ready-made SRMs for chemical quantification have rarely been used for SIMS quantification of boron in steels because of the heavy matrix effect arising from its significant difference of the microstructure despite their easy handling.

The authors tried to use a minimum number of SRMs for the born quantification in practically for unknown steels. Thus, the present work aims at quantifying of boron use within four ready-made SRMs and elucidating the matrix effect of the SRMs and FSW steels.

The steady-state equilibrium of the secondary ions could be established after 5 minutes of surface oxide removal by pre-sputtering. Also, the average values of the both intensities were obtained within the 50 numbers of maps.

Table 2 gives SIMS analytical conditions for resist anode encoder (RAE) image which will be used for retrospective depth profile later and raster depth profile, respectively. Furthermore, three different mass resolutions of M/ΔM 2000, 3500, and 4500 at two different secondary polarities, positive and negative 4.5 kV were used for the RAE image. The RSFs of four SRMs were measured initially from their relevant retrospective depth profiles of the RAE images. The RSFs linearity was then compared as a function of boron concentrations. The authors performed another attempt to set the comparison of RSFs. It was by using two types of a secondary ion species, the RSF_B of a cluster- polyatomic boron and the RSF_C of monatomic carbon as a function of boron concentration. The detection of single monatomic boron for RSF_B was not available under the negative secondary condition which was used in this study.

Table 2. SIMS analytical conditions

Item	RAE Image	Depth profile
Primary Ion	O_2^+	← same
Beam Mode	Scope mode	Raster mode
Field of view	150 um	63 um
$V_{Primary}$	12.5 kV	← same
$V_{Secondary}$	-4.5/+4.5 kV	-4.5 kV
$I_{Primary}$	50/500 nA	50 nA
M/ΔM	2000/3500/4500	4.5 kV
# of points (maps)	(50)	75

Figure 1 shows the optical micrograph of two different TMAZ of FSW steels with different contrasts in region 1 and region 2, respectively. It is not a chemical etched microstructure but a macro image. An elevated temperature of the rotating tool might be affected this abnormal contrast of the FSW steel surface.

The RSMs and FSW samples were machined 10 mm ×10 mm× 6 mm in size, followed by an epoxy mount and mirror polishing. Regions of interest were marked with a sharp edge diamond pencil.

Table 1. Chemical composition of the SRMs

SRM (NIST#)	C	Si	Mn	Ni	Cr	Al	B	Fe
1263A	0.62	0.74	1.5	0.32	1.31	0.24	9*	Bal.
1264A	0.87	0.06	0.25	0.14	0.06	-	110*	Bal.
1265A	67*	80*	57*	0.04	70*	7*	1.3*	Bal.
C1151A	340*	0.29	2.37	7.25	22.5	30*	10*	Bal.

Note: All units are wt.%, superscripts * indicate ppm.

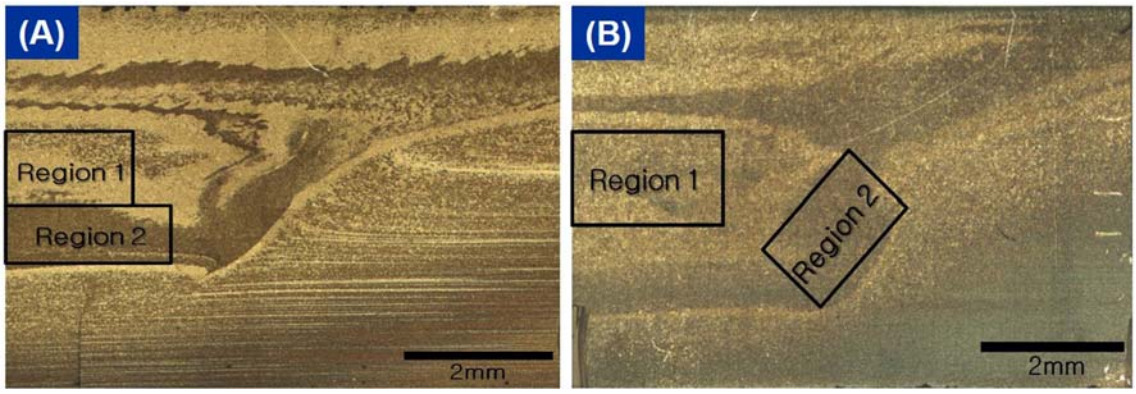

Fig. 1. Two FSW steels, (a) and (b) shows different contrast region at TMAZ.

In order to convert the RAE image to a retrospective depth profile, for a given species, the intensity for each data point of the retrospective depth profile was computed by the profiler using the following relationship,

$$I(t_n) = \frac{\sum_{i,j} P_n(i,j)}{T} \quad (1)$$

where, $P_n(i,j)$ is the pixel intensity in counts included in the contour for the *n-th* image planes, T is the integration time for each image, and t_n is the total time spent measuring from the beginning of the analysis to the end of the acquisition of the *n-th* image planes.

3. RESULTS AND DISCUSSION

3.1. RSF

Determination of RSF was made by the following equation.

$$RSF = \rho_i \frac{I_m}{I_i} \quad (2)$$

where, ρ_i is the impurity atom density in atoms/cm^3, I_i is the secondary ion intensity of impurity in cps, and I_m is the secondary intensity of the matrix in cps. The authors precisely described the process to determine the RSFs in the previous study [5].

The relative sensitivity factor for boron, and RSF_B, of the SRMs are calculated from their relevant RAE images and have been summarized in Table 3. Fig. 2 shows the variation of the RSF, (a) for negative secondary 4.5 kV and (b) for positive secondary 4.5 kV with different mass resolution, M/ΔM, as a function of corresponding boron concentration of SRMs. The red solid line rectangle (a) identified as SRM 1263 A, contains 0.24 wt% of aluminum. As mentioned in the previous study, this larger amount of aluminum, which was detected as $^{27}Al^{16}O$, is strongly interferes with $^{11}B^{16}O_2$ because it's mass is the same as 43. Whereas, the red solid line rectangle (b), identified as C1151A, which contains 22.6 wt% of chromium and 7 wt% of nickel. These results suggest us two things, (i) negative secondary polarity (Ps) is better for the detection of boron in the steel matrix, (ii) RSF is strongly affected by the matrix materials.

Table 4 summarized RSF_B and RSF_C which were calculated from a relevant map and depth profile using a different type of secondary species and mass resolution of the SRMs. RSF_B is obtained using $^{11}B^{16}O_2$ of cluster-polyatomic ion and RSF_C is obtained using ^{12}C of monatomic ion, respectively.

Figure 3 shows the variation of RSF_B and RSF_C as a function of corresponding boron concentration of the SRMs with different mass resolution. The best RSF stability was found in the raster depth profile at MR 4500. The relative standard deviation (RSD) of the RSF_B obtained by MR 2000 was

Table 3. Comparison of RSF_B calculated with different polarity and mass resolution (unit: atoms/cm^3)

P_S	M/ΔM	1263A	1264A	1265A	C1151A
	2000	1.67E17	4.85E17	1.01E18	8.01E17
-4.5 kV	3500	2.41E17	3.11E17	8.88E17	4.56E17
	4500	3.06E17	8.98E17	7.66E17	1.34E18
	2000	6.47E21	2.08E21	2.72E21	5.46E20
+4.5 kV	3500	7.17E21	3.38E21	1.31E21	3.99E20
	4000	5.95E21	1.68E21	7.50E20	2.54E20

Table 4. Comparison of RSF_B and RSF_C calculated with a different type of secondary ion species and mass resolution (unit: atoms/cm^3)

SRM	M/ΔM 2000		M/ΔM 4500
	Map/Retrospective DP		Raster DP
	RSF_B	RSF_C	RSF_B
1263A	7.88E18	2.37E19	1.12E19
1264A	3.55E19	2.14E22	2.29E19
1265A	2.48E19	1.56E20	2.13E19
C1151A	3.35E19	8.05E20	1.98E19
RSD	±21.4%	±82%	±12%

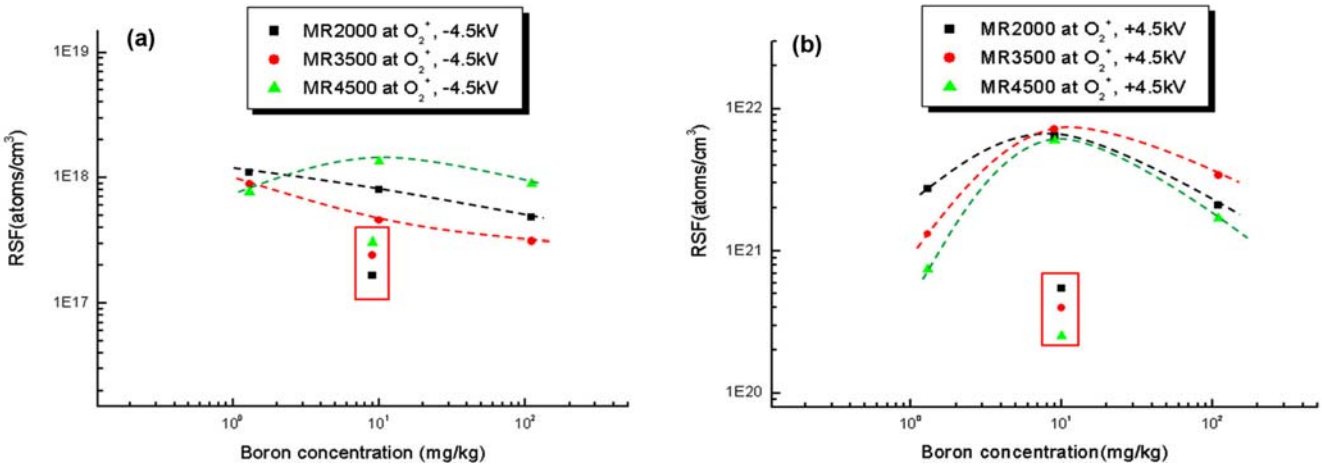

Fig. 2. Variation of RSF, (a) for negative secondary 4.5 kV and (b) for positive secondary 4.5 kV as a function of corresponding boron concentration of the SRMs with three different mass resolutions, M/ΔM.

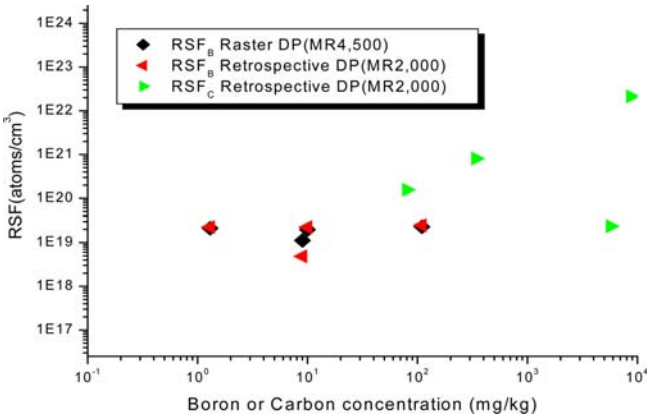

Fig. 3. Variation of RSF_B and RSF_C calculated with two different mass resolutions, M/ΔM, as a function of corresponding boron concentration of SRMs.

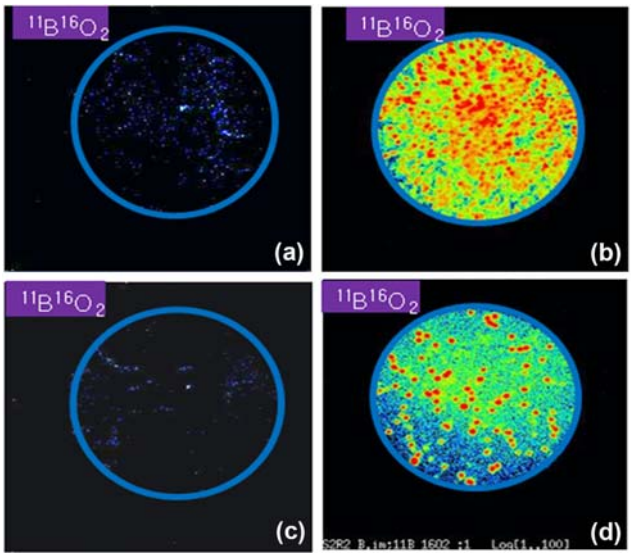

Fig. 4. RAE boron images of the TMAZ in FSW steel corresponding to Fig. 1. (a) #1 FSW, Region 1, (b) #1 FSW, Region 2, (c) #2 FSW, Region 1 and (d) #2 FSW, Region 2.

±21.4%, whereas it was ±12% when obtained by MR 4500. These results suggest us that the MR 4500 of the raster depth profile mode, black diamond in Fig. 3, will be more useful to reduce the aluminum interference than the retrospective depth profile mode. This could be explained by the difference of the sensitivity in each profile mode. The raster depth profile mode gives more secondary intensity than the retrospective depth profile. If SRM 1263A and high Al content SRM are excluded in the measurement then it can be further improved down to ±2.43% of the RSD.

3.2. Boron concentration in TMAZ in FSW steels

SIMS microscope boron images, detected as $^{11}B^{16}O_2$, of the TMAZ in FSW steels were obtained (Fig. 4). Boron could exist as several kinds of states such as precipitates of B_4C, $(Fe,Cr)_{23}(C,B)_6$, BN, or others. Regardless of the boron state, which may lead to segregation in the grain boundary or precipitation of different chemical species or soluble boron, the goal is to obtain an accurate determination of the total boron concentration with the corresponding boron ion map. The matrix effect arises not only by the boron state but also by the alloying elements and thermo mechanical treatment which will rather strongly contribute to the distinctive microstructure of iron and steels matrices. The smallest contrast aperture was needed for the best image resolution. One more important thing was the correction of the astigmatism which can arises from the aperture and slits. It must be carefully adjusted during all the measurements.

The FSW technique has been widely investigated in mostly low melting aluminum alloy. It was limited primarily to the application of the joining of steels and other high temperature materials by the absence of suitable tool materials that can operate at high temperatures [6]. Several works have been reported on the FSW of steel application [7-11]. The microstructure and mechanical property of the FSW joint depend on the FSW parameters as well as the base material. PCBN is the frequently used welding tool in the field of steel application as mentioned before. The two FSW steels have different contrast site by site in the TMAZ, the bright area of region 1 and the dark area of region 2 as shown in Fig. 1. Efforts to understand this contrast variation of the TMAZ in FSW joint steels was required to identifying the qualitative and quantitative distribution of the boron site by site.

Ozekcin *et al*. of ExxonMobil has been investigated the microstructure of FSW joint of API-grade carbon steels [12]. They used SEM, TEM and SIMS to investigate the qualitative comparison of the microstructure. They tried SIMS analysis in the TMAZ and TMAZ-HZ to compare the boron concentration. They revealed that the angular in morphology of the second-phase inclusion contains boron by SEM-EDS analysis which might be debris from the PCBN tool. Also, they suggested that some boron may have been dissolved in the solid solution in the TMAZ tried by the microprobe boron images of SIMS. But they didn't attempt a quantitative distribution of boron in the TMAZ of FSW steel.

Material flow and texture evolution in FSW aluminum alloy has been performed by Kang *et al.* [3]. They found that, during FSW, the microstructure of the material near the stir zone was found to be influenced by the rotational behavior of the tool pin.

The field of view, 150 um in diameter maps, displayed the qualitative distribution of impurity boron properly in the TMAZ. These maps were obtained using a counting time of 1.67 seconds for boron ion as $^{11}B^{16}O_2$ and matrix iron ion as $^{56}Fe^{16}O$. And the waiting time was sued, 0.56 seconds for $^{11}B^{16}O_2$ and 1.67 seconds for $^{56}Fe^{16}O$, respectively. A total of 50^{th} image plane was stored for one RAE map. It was taken in 3.3 min. One of the advantages of the RAE image is the

Table 5. Intensity ratio of the impurity and the matrix for the calibration curve of Fig. 5

SRMs	Retrospective Depth Profile (MR 2000)		
	I_i ($^{11}B^{16}O_2$) cps	I_m ($^{56}Fe^{16}O$) cps	I_i/I_m
1264A	8.02E3	4.13E3	1.94
1265A	1.57E2	4.98E3	0.0316
C1151A	7.77E2	3.00E3	0.259

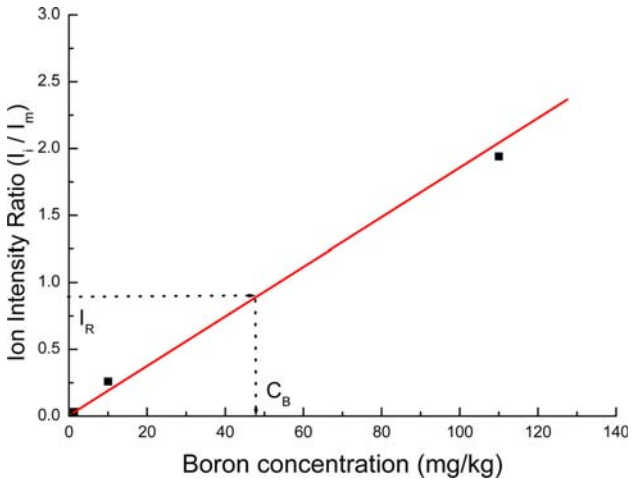

Fig. 5. Calibration curves of the SRMs for the quantification of boron in the TMAZ of FSW steels.

Table 6. The difference of the boron concentration of the TMAZ in FSW steels

TMAZ		I_i/I_m	Boron(ppm)
#1 FSW	Region 1	0.078	1.84
	Region 2	2.30	130.65
#2 FSW	Region 1	0.062	0.91
	Region 2	0.888	48.79

fast acquisition time. It shows that the region 2 of both TMAZ contains more boron than region 1 in Fig. 4.

The ratio of the ion intensity, I_i /I_m, namely I_i is the impurity boron intensity of $^{11}B^{16}O_2$ and I_m is the matrix intensity of $^{56}Fe^{16}O$, measured under identical experimental conditions. The ratio of the ion intensity is summarized in Table 5. The calibration curve obtained from Table 5 for FSW steels is shown in Fig. 5. The concentration of boron of TMAZ in FSW steels are now determined by taking the corresponding concentration value from the calibration curve in Fig. 5. The use of linear fit is recommended for the quantification. The final quantification results using the calibration curve is shown in Table 6.

4. CONCLUSIONS

The RSFs of boron in steel matrix were varied significantly by the polarity of secondary voltage and the matrix materials. The best RSF stability of boron in steel was found in the raster depth profile at MR 4500 and negative secondary voltage. Due to the shadow-off of the ion image map, the RAE ion map could not be applicable at MR 4500 [5]. However, the raster depth profile is available with the best reproducibility of ±12% at MR 4500 without ion image information. It is needed to find a compromise which is the main purpose of the SIMS investigation, impurity quantification or impurity imaging. A combination of cluster-polyatomic ion, $^{11}B^{16}O_2$ and $^{56}Fe^{16}O$ provided a good calibration curve with three SRMs. The boron concentrations of TMAZ in FSW steels were determined through the calibration curve by taking the corresponding boron concentration value (C_B) of the intensity ratio (I_i/I_m) from an unknown sample. A 150 um in diameter of ion maps clearly represented clearly the distribution of impurity boron in the TMAZ. This observation suggested that some boron may have been dissolved in the solid solution from the PCBN tool.

The new SIMS quantification technique developed by present authors is found to be effective for a more quantitative understanding of the wear mechanism of the PCBN tool in TMAZ of FSW steels.

ACKNOWLEDGMENTS

The authors would like to thank Jeffrey R. Shallenberger, Evans Analytical Group, MA & NJ, USA and Giovanni Cossu, Laboratory for Surface Science and Technology, ETH, Zurich, Switzerland for many helpful and thoughtful discussions.

REFERENCES

1. Ying Li, L.E. Murr, and J. C. McClure, *Mater. Sci. Eng. A.* **271**, 213 (1999).
2. T. Terasaki and T. Akiyama, *Welding in the World.* **47**, 24 (2003).
3. S. H. Kang, H. N. Han, K. H. Oh, J. H. Cho, C. G. Lee, and S. J. Kim, *Met. Mater. Int.* **15**, 1027 (2009).
4. W. Konig and A. Neises, *Wear.* **162**,12 (1993).
5. J. N, Kim, S. U. Lee, H. D. Kwun, J. W. Kim, K. S. Shin, and J. J. Lee, *Met. Mater. Int*. **18**, 361 (2012).
6. P. Threadgill and R. Johnson, *Proc. 14th Int. Offshore and Polar Eng. Conf.*, pp. 1-7, ISOPE, Toulon, France (2004).
7. T. J. Lienert, W. L.Stellwag, B. B. Grimmett, and R. W. Warke, *Welding Res. Supplt. to Welding J.* AWS, pp.1-5, (2003).
8. R. Johnson, J. Dos Santos, and M. Magnasco, *4th Int. Friction Stir Welding Symp.*,in CD-ROM, Park City, Utah, USA (2003).
9. P. Konkol, *4th Int. Friction Stir Welding Symp.,* in CD-ROM, Park City, Utah, USA (2003).
10. K. Okamoto, S. Hirano, M. Inagaki, S. H. C. Park, Y. S. Sato, H. Kokawa, T. Nelson and Sorenson, *4th Int. Friction Stir Welding Symp*., in CD-ROM, Park City, Utah, USA (2003).
11. M. Posada, J. DeLoach, AP. Reynolds, R. Fonda, and J. Halpin, *4th Int. Friction Stir Welding Symp.,* in CD-ROM, Park City, Utah, USA (2003).
12. A. Ozekcin, H. W. Jin, J. Y. Koo, N. V. Bangaru and R. Ayer, *Int. J. Offshore. Polar Eng.* **14**, 284 (2004).